# New Observations with CREAM

E. S. Seo[a,b] for the CREAM Collaboration
*(a) Inst. for Phys. Sci. and Tech., University of Maryland, College Park, MD 20742 USA*
*(b) Dept. of Physics, University of Maryland, College Park, MD 20742 USA*
Presenter: Eun Suk Seo (seo@umd.edu)

The Cosmic Ray Energetics And Mass (CREAM) balloon-borne experiment had its first flight from Antarctica. It made three circumnavigations around the South Pole for a record breaking duration of 42-days from 16 December 2004 to 27 January 2005. The balloon altitude stayed between 125,000 ft and 130,000 ft throughout most of the flight. The instrument has redundant charge identification and energy measurement systems capable of precise measurements of elemental spectra for Z = 1 - 26 nuclei over the energy range $\sim 10^{11} - 10^{15}$ eV to explore a possible limit to the acceleration of cosmic rays in supernovae. Measurements of the relative abundances of secondary cosmic rays (e.g., B/C) in addition to the energy spectra of primary nuclei will allow determination of cosmic-ray source spectra at very high energies. Preliminary results from the ongoing analysis are presented, and future plans are discussed.

## 1. Introduction

Indirect measurements from ground-based experiments have traced the all-particle spectrum from about $10^{14}$ eV to $>10^{20}$ eV. These measurements have shown that the energy spectrum above $10^{16}$ eV is somewhat steeper than the spectrum below $10^{14}$eV, with the so-called spectral "knee" between these energies. Whether and how the knee structure is related to the mechanisms of particle acceleration, propagation, and confinement are among the major current questions in particle astrophysics.

The CREAM experiment [1] was designed and constructed to extend balloon and space-based direct measurements of cosmic-ray elemental spectra to the highest energy possible in a series of balloon flights.

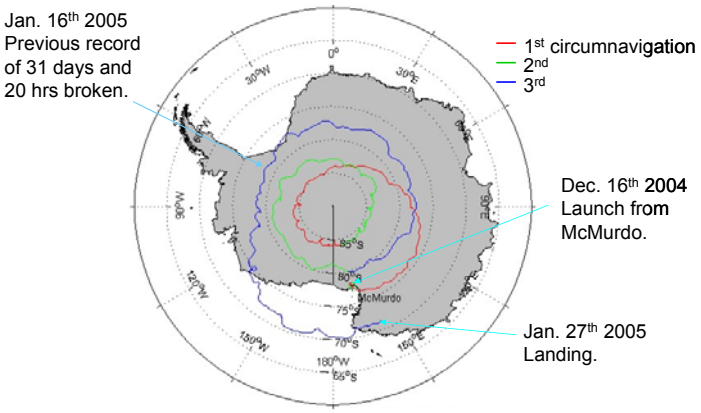


**Figure 1.** Balloon trajectory of the CREAM flight. CREAM broke both distance (~14,000 nautical miles) and duration (41 days 21 hrs 36 mins) records for a long duration balloon (LDB) flight.

The detailed energy dependence of elemental spectra at very high energies, where the rigidity-dependent supernova acceleration limit could be reflected in composition change, provides a key to understanding the acceleration and propagation of cosmic rays. Simultaneous measurements of secondary and primary nuclei allow determination of the source spectra at energies where measurements are not currently available.

## 2. Balloon Flight

The CREAM payload was successfully launched from McMurdo, Antarctica on 16 December 2004, and it subsequently circumnavigated the South Pole three times. As shown by the trajectory in Figure 1 and latitude in Figure 2, the balloon drifted toward the pole, made a full circle around latitude 85°S, and gradually spiraled northward. The flight was terminated on 27 January 2005 after a record-breaking duration of 42-days. The payload landed on the high plateau 410 nautical miles northwest of McMurdo station. The balloon float altitude was between 125,000 and 130,000 ft (38 and 40 km) throughout most of the flight as shown in Figure 2. The corresponding average atmospheric overburden was only ~3.9 g/cm$^2$. The diurnal altitude variation due to the Sun angle change was very small, < 1 km, near the pole, i.e. at high latitude, which increased as the balloon spiraled out to lower latitudes. The temperature of the various instrument boxes stayed relatively constant with daily variation of about 1 – 3 °C, consistent with the Sun angle.

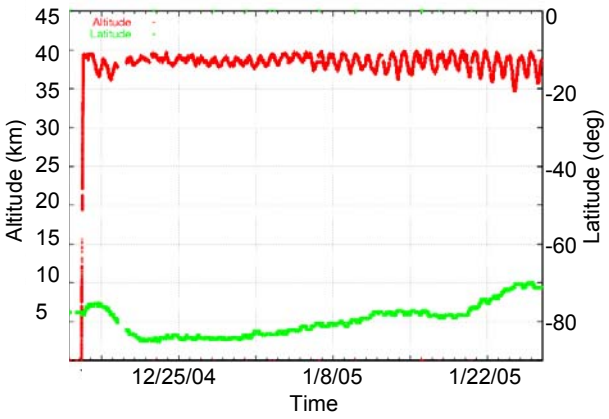


**Figure 2.** Altitude and latitude of the balloon.

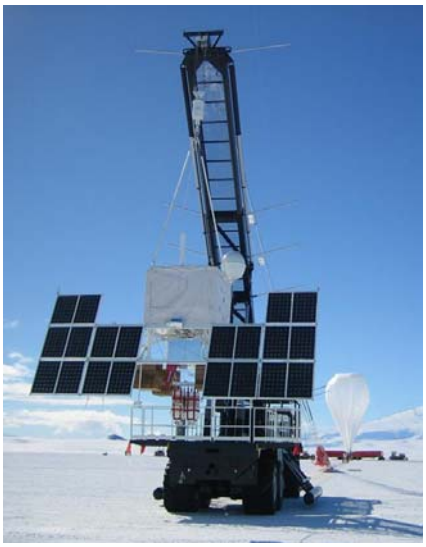

**Figure 3.** CREAM ballooncraft at the launch site while the balloon is being inflated.

All of the high energy data ( > ~ 1 TeV) were transmitted via Tracking and Data Relay Satellite System (TDRSS) during the flight, while the lower energy data were recorded on board. A total of 60 GB of data (~ 40 × 10$^6$ science events) were collected. The flight operation was unique in several aspects. First, this was the first long duration balloon (LDB) mission to transmit all the prime science and housekeeping data (up to 85 kbps) in near real-time through the TDRSS via a high-gain antenna, in addition to having an onboard data archive. To fit the data into this bandwidth, science event records excluded information from channels that had levels consistent with their pedestal value. This so-called 'data sparsification' reduced the average high energy shower event record size by nearly 95%. Second, the instrument was shipped to Antarctica fully integrated to minimize the flight preparation time. The crew became

flight ready 2 weeks after the arrival in Antarctica. Third, the science instrument was controlled from the home institution throughout the flight as soon as line-of-sight ended at the launch site.

As the balloon drifted away from the line-of-sight, which lasted for ~12 hours after launch, commanding was transferred off the continent to the Science Operation Center at the University of Maryland. Primary command uplink was via TDRSS, with Iridium serving as backup whenever the primary link was unavailable due to schedule or traversing zones of exclusion. The nearly continuous availability of command uplink and data downlink throughout the flight allowed a rapid response to changing conditions on the payload (e.g., altitude dependent effects). See References [2, 3, 4] for more details of the flight operation and CREAM data acquisition system.

The CREAM balloonicraft [1], referring to all hardware below the attachment point to the mobile launch vehicle, shown in Figure 3, is an integrated assembly of the science instrument and support systems mounted on the primary support structure. The science instrument was not pressurized, and it was supported by the Command and Data Module (CDM) developed by the National Aeronautics and Space Agency (NASA) Wallops Flight Facility (WFF) [5]. This is in contrast to typical LDB payloads which utilize the Support Instrumentation Package (SIP) provided by the Columbia (formerly National) Scientific Balloon Facility (CSBF). The 40 MCF-lite balloon carried a total suspended weight of 6000 lb, including ~2900 lb for the science instrument and support structure, and ~1100 lb of ballast. The large amount of ballast played an important role for the zero pressure balloon to keep its high altitude throughout the flight, especially during the third circumnavigation when it drifted northward. The science instrument power consumption was ~400 W. Both the science instrument and the flight support systems were developed for nominal 100-day ultra-long-duration balloon (ULDB) missions.

## 3. Instrument

An exploded schematic view of the instrument designed to meet the CREAM measurement objectives is shown in Figure 4. See Reference [1] for the instrument details. A suite of particle detectors are employed to determine the charge and energy of the very high energy particles. They include a Timing Charge Detector (TCD), a Transition Radiation Detector (TRD) with a Cherenkov Threshold Counter (CTC), and a calorimeter module comprised of a Silicon Charge Detector (SCD), a carbon target, scintillating fiber hodoscopes (S0/S1 and S2), and a stack of tungsten plates with interspersed scintillating fiber layers. Multiple charge measurements with the TCD, CTC, SCD, and

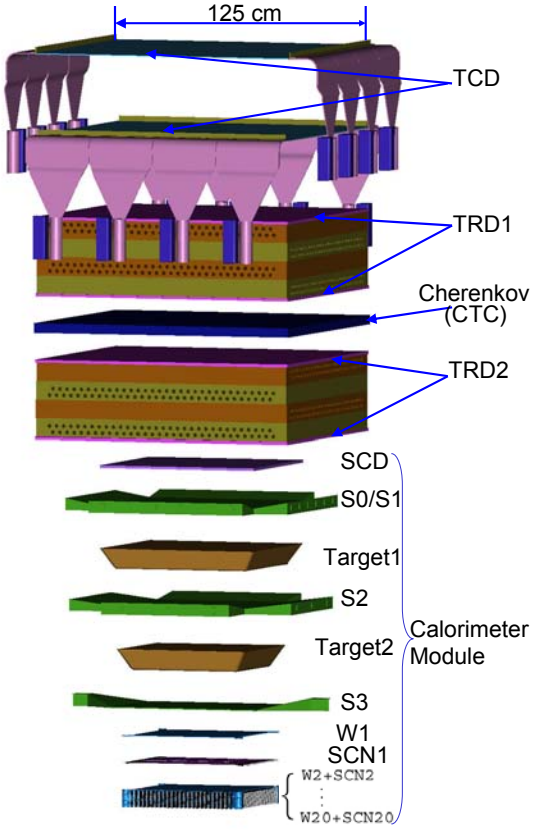


**Figure 4**. Schematic of the CREAM instrument.

S0/S1 layers of scintillating fibers accurately identify the incident particles by minimizing the effect of backscattered particles from the calorimeter. The TCD utilizes the fact that the incident particle enters the TCD before developing a shower in the calorimeter, and the backscattered albedo particles arrive several nanoseconds later. A layer of scintillating fibers, S3, located between the carbon target and the tungsten calorimeter provides a reference time. The SCD is segmented into pixels to minimize multiple hits of backscattered particles in a segment.

The carbon target induces hadronic interactions in the calorimeter module, which measures the shower energy and provides tracking information to determine which segment(s) of the charge detectors to use for charge measurement. Tracking for showers is accomplished by extrapolating each shower axis to the charge detectors. The hodoscopes S0/S1 and S2 provide additional tracking information above the tungsten stack. Tracking for non-interacting particles in the TRD is achieved with better accuracy (1 mm resolution with 67 cm lever arm, 0.0015 radians). The TRD determines the Lorentz factor for $Z > 3$ nuclei by measuring transition x-rays using thin-wall gas tubes. The TRD and calorimeter, which can also measure the energy of protons and He, have different systematic biases in determining particle energy. The use of both instruments allows in-flight cross-calibration of the two techniques and, consequently, provides a powerful method for measuring cosmic-ray energies. As illustrated by the example of a ~10 TeV Fe event in Figure 5, the instrument functioned well during the flight. The CREAM trigger aperture is fairly large with an acceptance of ~2.2 $m^2sr$.

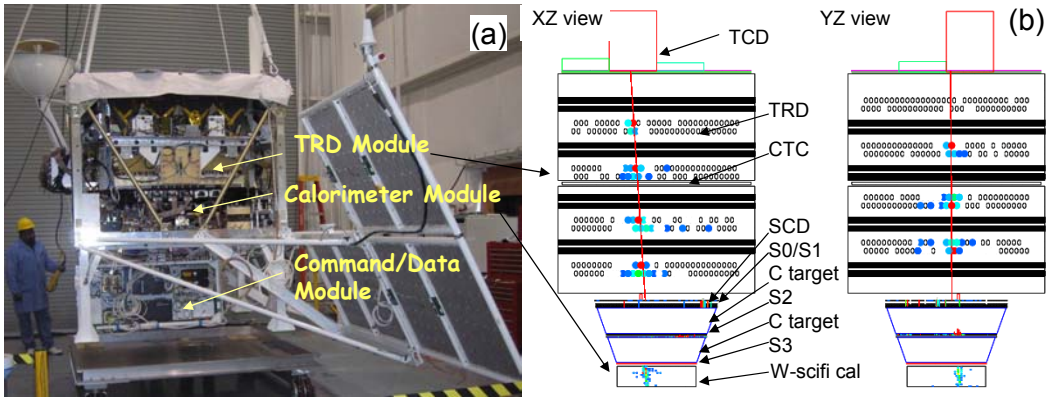


**Figure 5.** CREAM Instrument: (a) Photograph; (b) Event display; A cosmic-ray Fe nucleus with estimated energy 10 TeV entered the instrument to give a large signal (red box at the top) in the TCD, a clear track in the TRD (blue and red filled circles), a large signal in the SCD (red box) and a well-defined shower in the calorimeter (light blue).

### 3.1. Timing Charge Detector

The TCD [6, 7] is made of two layers of 5 mm-thick 1.2 m × 0.3 m plastic scintillators, read out with fast timing photomultiplier tubes via twisted-strip adiabatic light guides and pipes. It is used to measure the scintillation signal generated by incident cosmic rays to determine their charge with sufficient accuracy (~0.2*e* for O to ~0.35*e* for Fe) to resolve individual elements. The TCD operated well throughout the entire length of the flight. One of 18 photomultiplier tubes in the TCD system failed near the end of the flight.

The TCD has four gain ranges corresponding to signals derived from the various photomultiplier dynode feeds. Each of these is targeted at a range of elements. Figure 6 shows a distribution of energy deposited per unit pathlength in the TCD scintillators derived from the mid-level gain range as a function of the light yield

per unit path-length from the Cherenkov detector. This TCD gain range is targeted at 'L/M' nuclei. These events were selected from the first day of the flight by restricting the geometry to the central parts of these counters.

The clear populations of the signals due to B, C, N and O nuclei show the expected charge resolution for heavy nuclei. After mapping corrections have been applied a similar resolution is possible across the entire aperture. Good separation between B and C is very important for accurate measurements of secondary nuclei. These preliminary data show that the instrument has sufficient charge resolution to allow efficient use of B and C events for determination of the abundance ratio of secondary to primary nuclei. The Cherenkov trigger threshold is clearly visible in Figure 6, and relativistic B nuclei are well above threshold. Also visible are the abundant lower energy events due to the low geomagnetic rigidity cutoff over Antarctica, which produce higher ionization loss and a lower Cherenkov signal. Signals from heavier cosmic rays up to Fe are also present in the flight data, but they appear in different TCD gain ranges from that shown in Figure 6. Using the Cherenkov data, relativistic particles were selected to obtain the charge histogram in Figure 7. Note that not all corrections are made, so the event selections are preliminary. This plot is only indicative of charge resolution, and the relative abundances are not meaningful.

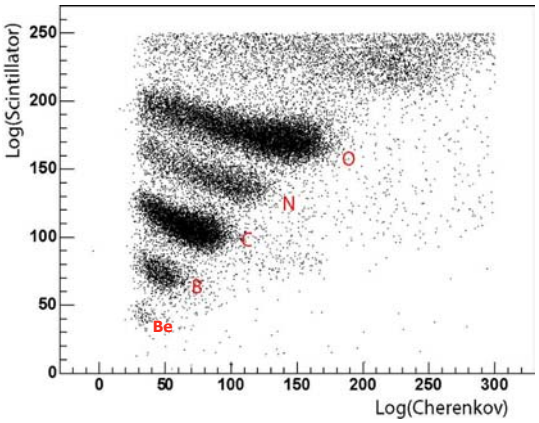


**Figure 6.** Measured energy losses in the TCD scintillator versus Cherenkov light signal for a short (~1 day) portion of the flight. B, C, N and O nuclei populations are clearly visible.

3.2. Transition Radiation Detector

The TRD [7] consists of eight layers of polystyrene foam radiator combined with a total of 512 thin-walled proportional tubes, each 2 cm in diameter and 1.2 m long. They are filled with a mixture of xenon (95%) and methane (5%) gas at a pressure of 1 atmosphere. The tubes are arranged in 16 layers, and the pattern of hits in the tubes due to nuclei traveling through them is analyzed to reconstruct the particle's trajectory in three dimensions. The Lorentz factor (γ of a heavy nucleus can be determined from the energy loss per unit path-length in the TRD gas. In the region from minimum ionizing to ~500 GeV/n, this is provided by the logarithmic relativistic increase in ionization loss, which is large (~1.6) for xenon gas. At higher energies, above 1 TeV/n, significant transition radiation is produced in the radiator material and accompanies the direct particle energy losses, providing an additional logarithmic rise in response until saturation sets in near γ ~20,000. The response of this TRD has beenwas calibrated in a CERN test beam in 2001 [38].

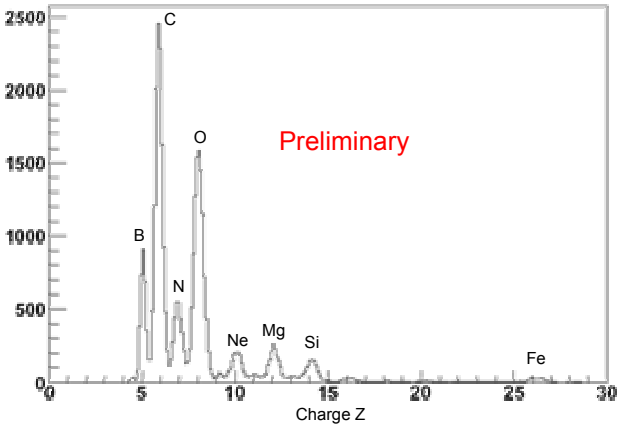


**Figure 7.** TCD charge distribution.

The loss rate of the xenon mixture from the TRD gas system was very low and amounted to only ~10 % of the system volume over the 42-day flight, even though this gas was contained in a total of ~0.6 km of 100 μm wall thickness tubing at an over pressure of 1 atmosphere. This leak rate was slow enough that periodic redistribution of the gas already in the system every few days was sufficient to maintain good response from all layers. No top-off from the onboard gas reservoir was needed. Perhaps more remarkable was the stability of the signal response using the same gas for over 40 days. The proportional counter resolution did not noticeably degrade during the flight, even though no fresh gas flowed through the tubes. Similar assemblies with an over pressure operated at ground level typically lose resolution even after 12 hours or so. This suggests that diffusion of electronegative oxygen into the tubes is the most likely culprit for this gradual degradation of resolution with time observed in the lab. The oxygen concentration at balloon altitudes is low enough that the rate of this effect is at least 100 times slower.

For the same event subset used in Figure 6, Figure 8 shows a preliminary distribution of energy deposited per unit pathlength in the proportional tubes along the particle trajectory as a function of light from the Cherenkov detector. Populations of events due to B, C, N, O, Ne, Mg, Si, and Fe nuclei are clearly visible. The TRD signal is derived from a dual-gain range system using Amplex 1.5 ASICs with an effective dynamic range of 12 bits. The resulting TRD and Cherenkov signal systems are quite linear over the entire dynamic range. The high energy events will ultimately be derived from those that are relativistic in the Cherenkov and have a large signal in the TRD for a given charge.

### 3.3. Cherenkov Threshold Counter

The Cherenkov detector is a 1 cm-thick 1.2 m × 1.2 m plastic radiator sheet doped with blue wavelength shifter. This is viewed along the edges by eight small photomultiplier tubes via plastic wavelength shifting bars, which capture the blue light produced in the radiator and shifts it into the green region. This technique provides a compact detector with uniform response. The measured variations of light collection with position in this device during the flight are < 15 %. The Cherenkov detector is inserted between the two sections of the TRD, as shown in Figure 4. This is used to identify relativistic nuclei, which is important because of the high flux of unwanted low-energy particles at Antarctic latitudes. The Cherenkov detector also provides a determination of the incident cosmic-ray charge that is complementary to the TCD measurement. The heavy nucleus trigger of CREAM is set by thresholds in the TCD and Cherenkov detectors. During the flight these were adjusted so that a vertical relativistic Boron nucleus is well above these thresholds.

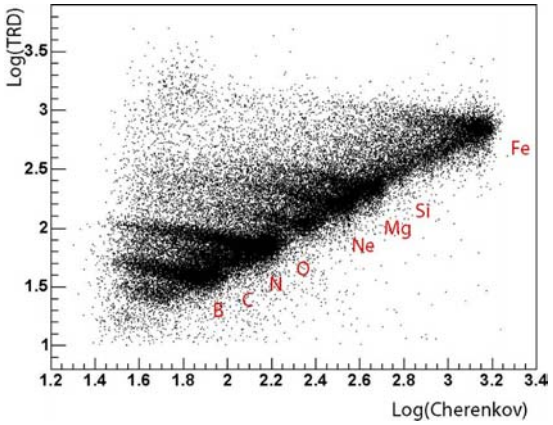


**Figure 8:** Measurements of the energy deposited in the TRD tubes versus the normalized Cherenkov light signal during ~1 day of the flight.

### 3.4. Silicon Charge Detector

The SCD [9, 10] consists of 26 ladders, each holding seven silicon sensor modules with associated analog readout electronics [11]. The sensors are slightly tilted and overlap each other in the x- and y- directions, providing full coverage in a single layer, with a 79 × 79 $cm^2$ area. The silicon sensors were fabricated from

380 μm thick, 5" diameter silicon wafers. Each sensor is divided into a 4 × 4 array of 2.12 $cm^2$ pixels. The readout electronics are designed around a 16-channel CR-1.4A ASIC for each sensor, followed by 16 bit ADCs, allowing fine charge resolution over a wide dynamic range covering up to Z = 33 signals. The total power consumed for the readout and control electronics is about 50 W. Copper thermal straps are attached to the cover in order to keep the detector within its operational temperature range. The housekeeping data show that the detector temperature fluctuated as the payload altitude changed, but remained within the operational limits. Pedestal values were periodically measured for all channels, in order to allow offline corrections for variations caused by temperature changes. Dead or noisy channels, 3.7% of all channels, were masked in sparsifying the data during the flight. To remove coherent changes, 26 channels were recorded for all events.

Analysis of the SCD data begins with the tracking information for incident cosmic rays obtained from the TRD and/or calorimeter. For events triggered by high-Z cosmic rays, tracks that are well reconstructed in the TRD are extrapolated to the plane of the SCD. Reconstruction errors in the track angle and offset are considered in defining the search region in the SCD when looking for a matched hit. After subtracting pedestal values, the SCD pixel with the maximum signal in the search area is selected as a candidate. The SCD hit is finally selected if the distance between the track intersection with the SCD plane and the candidate pixel is less than 60 mm. The SCD signal is then corrected for the track angle with respect to the sensor plane. Using the correlation between the reconstructed charge signals from the SCD and the Cherenkov counter, as done for the TCD, relativistic particles are selected. High energy charge-1 and charge-2 events triggered by the calorimeter are analyzed similarly, using the reconstructed shower information. The resulting SCD charge histograms are shown in Figure 9. Charge peaks for major elements are separated clearly in the SCD. Note that the relative abundance shown in these figures are not corrected for detector efficiencies or acceptance.

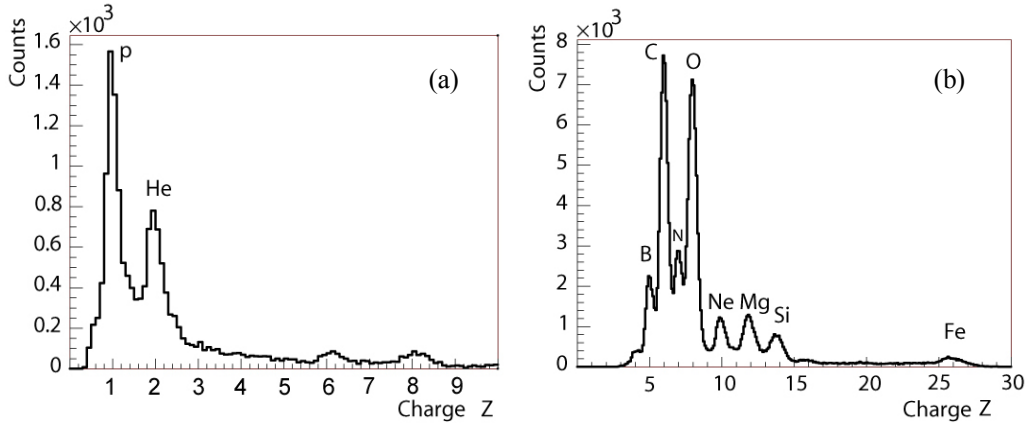


**Figure 9.** Preliminary flight data: SCD charge histograms for both (a) Low-Z trigger and (b) High-Z trigger events show clear charge separation for the major elements. The relative abundance has no significance in these plots.

### 3.5. Fiber hodoscopes

There are 3 hodoscopes in the instrument. The S0/S1 hodoscope pair, located above the graphite target layers, has 4 crossed layers of 2 × 2 $mm^2$ scintillating fibers. Each layer is comprised of 360 tight-packed fibers. The third hodoscope, S2, located between the two graphite targets, is constructed in a manner similar to S1, but with shorter scintillating fibers: the active area is only 63 × 63 $cm^2$ compared to 79 × 79 $cm^2$ for

S0/S1. All three hodoscopes facilitate improved track reconstruction, with fitting points relatively far above the thin calorimeter, thereby improving the lever arm for track fitting [12]. The S2 hodoscope also indicates whether the first interaction occurred in the upper or lower carbon target section. Figure 10 shows clear correlation between S0/S1 and SCD charge measurements. The S0/S1 calibration is preliminary.

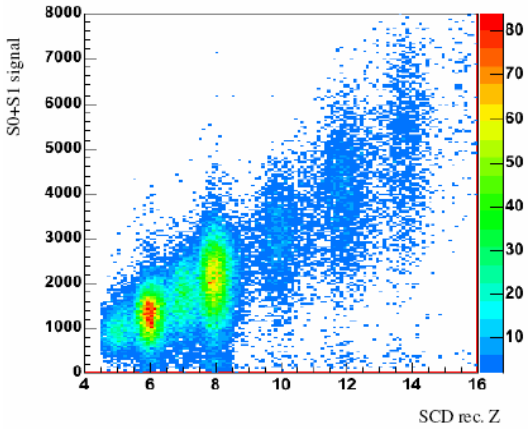


**Figure 10.** Correlation between hodoscope and SCD. charge measurements

### 3.6. Calorimeter

The calorimeter [13, 14, 15] combines a 0.5 $\lambda_{int}$ thick graphite target and a stack of 20 tungsten plates, each 3.5 mm (1 $X_0$) thick, followed by a layer of 0.5 mm diameter scintillating fibers grouped into fifty 1 cm-wide ribbons. The calorimeter fibers are read out through 73-pixel hybrid photo diodes (HPD) to transform light signals to electrical signals that are then digitized, and sparsified to remove signals that are likely to be pedestals. Real signals are transferred to the science flight computer to be incorporated into event records. The signal is optically split into low-, mid- and high-energy ranges, with progressively smaller fractions of the light signal, and with the mid- and high-range attenuated using neutral density filters with transmission coefficients of 50% and 16%, respectively. This arrangement allows the front end electronics to cover the 1:200,000 dynamic range between the smallest shower signal of interest and the highest single-ribbon signal expected in a 1000 TeV shower. The low- and mid-range signals of each ribbon are read out by separate pixels, while the high-range signals are read out in groups of five, for a total of 2200 channels. The HPD dynamic range is ~1:1,000,000, and does not constrain the readout linearity. During event reconstruction the different ranges are inter-calibrated for each ribbon separately. Figure 11 shows an example of such a ratio of low- and mid-range signals for one ribbon. Such plots were used to inter-calibrate the different ranges for each ribbon, in order to obtain measurements from the mid- range wherever the low-range was saturated. This calorimeter readout system, sensitive down to about 5 MeV per ribbon, has been successfully calibrated at CERN using electron beams. In flight, LED flasher events monitor the HPD's, while injection of predefined amounts of charge monitor the readout chains.

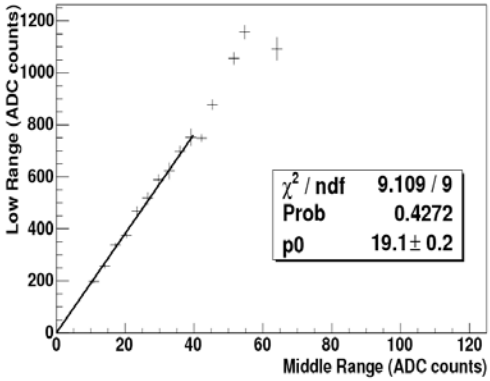


**Figure 11**. An example of the low-range vs. mid-range signals measured from the same fiber ribbon during the flight. A solid line represents a linear fit.

During the flight, the calorimeter trigger was set to require at least 6 consecutive layers with a threshold of ~60 MeV. This provided nearly 100% efficiency for showers of protons above 3 TeV (estimate based on Monte Carlo study). Figure 12 shows a preliminary result of the calorimeter energy deposit distribution for events recorded with a calorimeter trigger. The energy deposit was reconstructed using a preliminary set of

calibration constants from beam calibration, LED-based HV gain corrections, and flight measurements of the ratios between different optical ranges. A deposit of about 3.2 along the horizontal scale in Figure 12 corresponds to incident energy ~1 TeV, close to the calorimeter threshold. This energy deposit gives a quick check of the energy spectrum, which in this case shows a reasonable power law, and shows that we have data extending well above 100 TeV.

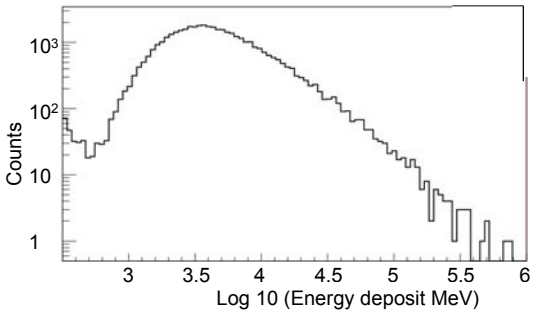


**Figure 12**. Preliminary calorimeter energy deposit distribution.

## 4. January 20 solar flare

It should be noted that CREAM was afloat and taking data during the January 20 solar flare [16]. While the calorimeter and TRD were not designed to measure energies as low as solar flare particles, and the instrument was not triggered by these low energy particles, they were recorded during periodic pedestal runs of the SCD and hodoscopes. As shown in Figure 13, a sudden increase in readout levels during pedestal runs of the SCD, and hodoscopes S0, S1, and S2 coincided with the reported powerful solar flare and the spike in the GOES-11 proton flux. The counts decrease with depth in the instrument, consistent with an

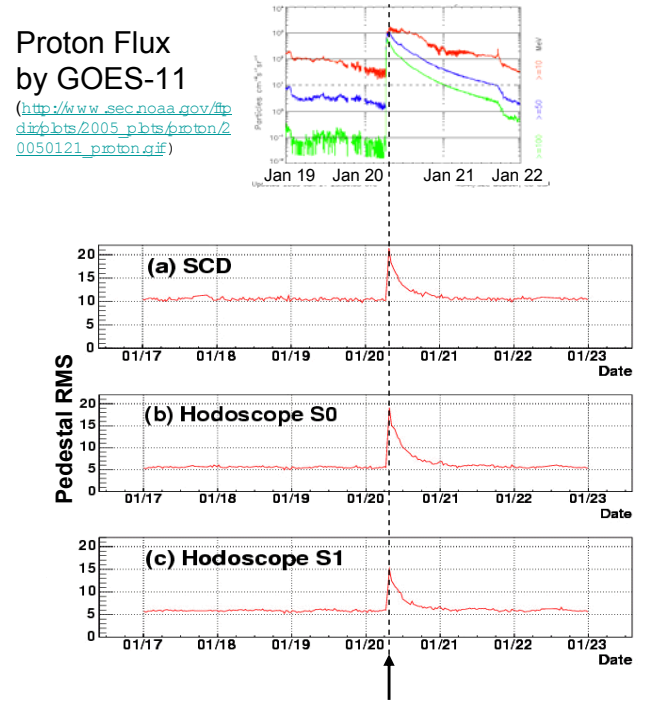


**Figure 13.** Sudden increase in readout levels during pedestal runs occurred at about 7am on Jan 20 (GMT). This coincided with a reported powerful solar flare.

energy spectrum that decreases with increasing energy of incident particles. Our plan is to select the SCD pixel with the highest signal for each event to determine the particle charge. We will also try to estimate the energy by checking signals in layers of detectors at different depths, SCD, S0, S1 and S2 since different energy particles will range out at different depths.

## 5. Expected Results

The data collected in this ~ 42-day flight will be adequate for accomplishing two significant measurement objectives. It will (1) measure secondary nuclei in the cosmic ray flux with elemental resolution and with high statistical accuracy up to energies of ~500 GeV/n and (2) extend the spectral measurements of primary nuclei, e.g., p, He, C, N, O, Ne, Mg, Si, and Fe, to higher energies and resolve differences in those spectra reported by various experiments such as ATIC, JACEE, and RUNJOB.

Figure 14 shows the abundance of the secondary nucleus Boron relative to Carbon, its most likely progenitor nucleus. The diamond and cross symbols show data collected, respectively, from the HEAO [17] and CRN [18] space instruments in the 1980's. There is a clear lack of accurate measurements above ~40 GeV/n. Also shown on this plot are curves for how the propagation path-length might vary with energy as $E^{-\delta}$, with $\delta$ = 0.33, favored in reacceleration models, or $\delta$ = 0.6, used in a standard leaky box model. The accurate measurement of $\delta$ is crucial for determining the cosmic ray *source* spectral index. If $\delta$ = 0.6, the source index is close to 2.1, but it could be as steep 2.4 if $\delta$ = 0.33.

The CREAM data at high energies should resolve these issues. Because of the strong relativistic rise in the specific ionization loss in xenon gas, the TRD is capable of measuring the B/C ratio as a function of energy below the region of significant TR production, specifically in the region above ~10 GeV/n. This relativistic rise provides a response factor of ~1.7 between minimum ionizing and ~500 GeV/n. The coupling of this effect with the excellent resolution of the TRD gas tubes for measuring specific ionization of heavy nuclei (for example $\sigma$ ~ 8% for Boron nuclei), provides an energy resolution in this region of $\sigma_\gamma/\gamma$ ~ 20%, where $\gamma$ is the Lorentz factor. The potential of the CREAM measurement is shown as filled circles in Figure 14. These indicate the level of statistical quality expected over a wide range from 10 GeV/n to 500 GeV/n with an assumed level of the B/C ratio lying between the two model calculations. These potential measurements would be the first major extension of our knowledge of the B/C ratio at high energy in over a decade. Clearly the two models shown can easily be distinguished with these statistics. Also shown is the expected production level by spallation interactions in 5 g/cm$^2$ of atmosphere above the balloon instrument: the average flight altitude was actually ~3.9 g/cm$^2$. While this background may ultimately limit balloon

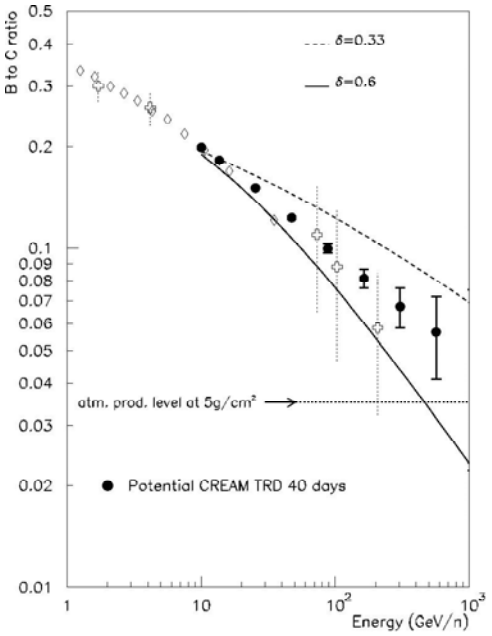


**Figure 14.** The B/C ratio vs. energy together with potential CREAM measurements on a ~ 42 day flight. The model curves are discussed in the text.

measurements at very high energies, it is small compared to the expected B/C ratio from spallation in the interstellar medium below ~500 GeV/n.

Accurate spectral measurements of both secondary and primary cosmic rays are essential for understanding cosmic ray propagation. The energy spectra of primary cosmic rays are known with good precision up to energies around $10^{11}$ eV, where magnetic spectrometers have been measuring spectra. Above this energy the composition and energy spectra are not accurately known, although there have been some pioneering measurements [18, 19, 20]. Precise measurements are needed to clear up some conflicting reports. For example, Asakimori et al. [19] reported a difference in the spectral indices for p and He, but Apanasenko et al. [20] did not see such a difference. An increase in the flux of helium relative to protons could be interpreted as evidence for two different types of sources/acceleration mechanisms for H and He [21]. A bend in the proton spectrum was reported to occur near 2 TeV [22], and a different study indicated a bend around 40 TeV [23]. These roll-off energies for protons are 1 - 2 orders of magnitude below the "knee" seen in the all-particle spectrum. There also seems to be an overall trend for the spectra of heavier elements to become flatter with increasing energy. Specifically, the spectral slopes at higher energies seem to be close to values around 2.5 to 2.6, which is significantly flatter than the low energy slopes around 2.7.

Figure 15a shows compiled proton and helium spectra. Among the many magnet spectrometer data sets at low energies, only the most recent space-based AMS data [24] are shown. Data from the Balloon-Borne Experiment with a Superconducting Solenoid – BESS [25], not shown, are consistent with the AMS results. Recent data from ATIC [26], with its (much-deeper-than-JACEE) fully-active calorimeter, which contains the electromagnetic shower maximum, are in better agreement with the space-based and balloon-borne magnet spectrometer data than old calorimeter measurements [27] at lower energies. While the proton flux reported by ATIC and JACEE [19] are similar, the He flux from ATIC is lower than the JACEE flux at high energies. JACEE reported a significantly smaller p/He ratio, ~12.5, compared to ~20 at lower energies. The ATIC data, which fills the gap between the magnet spectrometer measurements at low energies and the emulsion measurements at higher energies, show a ratio close to the magnet spectrometer measurements of ~20. Assuming the same spectral shape as ATIC, the CREAM measurement capability from a ~ 42-day flight is shown with filled squares. The first CREAM flight, with collection factor about twice that of ATIC for p and He, will extend precision measurements to higher energies and clearly resolve the discrepancies reported by prior experiments.

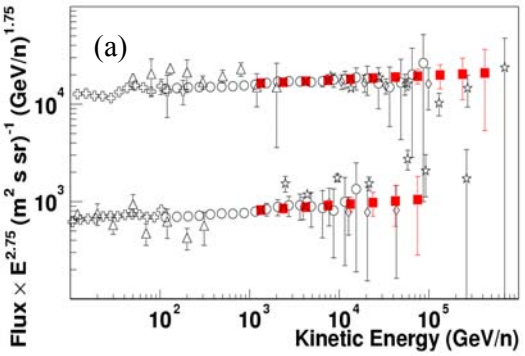


**Figure 15a.** Comparison of potential proton (upper) and He (lower) data from a ~ 42-day flight of CREAM (filled squares) with Ryan et al. (open triangles), JACEE (open stars), AMS (open crosses), and ATIC (open circles) results.

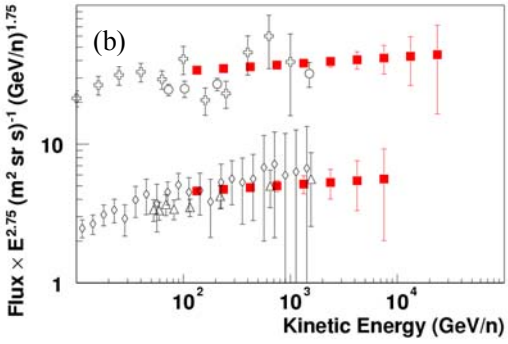


**Figure 15b.** Comparison of potential O (upper) and Fe (lower) nuclei spectra from a ~ 42-day flight of CREAM (filled squares) with prior measurements: Simon 1980 (crosses); Müller 1991 (circles, triangles); Ichimura 1993 (diamonds).

The CREAM TRD provides a collection factor about 10 times that of ATIC for Z > 3 nuclei, so it will also provide pioneering new data on heavy nuclei spectra. Figure 15b compares the O and Fe data expected from a ~ 42-day flight of CREAM with results from the CRN instrument [18]. Additional high quality data for O, Fe, and other heavy nuclei from the successful ~ 10-day flight of TRACER during the FY 2004 austral summer were presented at this conference [28, 29], but the instrument threshold at oxygen precluded its measurement of the B/C ratio.

## 6. Status Summary

The CREAM instrument was designed and constructed to meet challenging requirements of ultra long duration balloon flights, and it was calibrated in a series of beam tests at the CERN SPS before the flight. The science instrument, support systems, and operation scheme were successfully tested for ultra-long-duration flight throughout the record-breaking LDB flight. With excellent particle charge and energy resolutions, and relatively large collection factor, each CREAM flight will extend the reach of precise composition measurements to energies not previously possible. It is possible to conduct annual flights by alternating two science instrument suites, CREAM-I and CREAM-II, since the same instrument cannot be flown in consecutive years due to the time required for recovery, return to the laboratory, and refurbishment. The CREAM-I instrument was fully recovered with Twin Otter airplane flights after its record-breaking flight, and it is being refurbished in anticipation of another launch in 1 - 2 years. The CREAM-II instrument and the refurbished support system were integrated for launch in September 2005. The successful internal and external hang tests were followed by 24 hr burn-in for 5 days. The flight crew and science team are currently in Antarctica preparing the balloonicraft for another successful launch in December 2005.

**Figure 16**. A photograph of CREAM payload at the landing site and a twin otter plane used for the recovery.

**Figure 17**. CREAM-II instrument completed hang test at NASA WFF and shipped to Antarctica for its flight in December 2005.

## 7. Acknowledgements

This work was supported by NASA research grants. The authors thank NASA/WFF, Columbia (formerly National) Scientific Balloon Facility, National Science Foundation Office of Polar Programs, and Raytheon Polar Service Company for the successful balloon launch, flight operations, and payload recovery.

## References


[1] E. S. Seo et al., Adv. in Space Res., 33/10, 1777 (2004); http://cosmicray.umd.edu/cream/cream.html.
[2] Y. S. Yoon et al., Proc. 29th ICRC, Pune, 3, 429 (2005).
[3] S. Y. Zinn et al., Proc. 29th ICRC, Pune, 3, 437 (2005).
[4] S. Y. Zinn et al., Nucl. Instrum. Methods A, in press (2005).
[5] W. V. Jones et al., Proc. 29th ICRC, Pune, 3, 405 (2005).
[6] J. J. Beatty et al., Proc. of the SPIE 4858, 248 (2003).
[7] S. Coutu et al., Proc. 29th ICRC, Pune, 3, 393 (2005).
[8] P. J. Boyle et al., Proc. 28th ICRC, Tskuba, 2233 (2003).
[9] J. M. Yang et al., Proc. 29th ICRC, Pune, 3, 345 (2005).
[10] I. Park et al., Proc. 29th ICRC, Pune, 3, 341 (2005).
[11] I. Park et al., Nucl. Instrum. Methods A, 535, 158 (2004).
[12] P. S. Marrocchesi et al., Nucl. Phys. Proc. Suppl. 134, 75 (2004)
[13] M. H. Lee et al., Proc. 29th ICRC, Pune, 3, 409 (2005).
M. H. Lee et al., Proc. 29th ICRC, Pune, 3, 413 (2005).
M. H. Lee et al., Proc. 29th ICRC, Pune, 3, 417 (2005).
[14] P. S. Marrocchesi et al., Proc. 29th ICRC, Pune, 8, 109 (2005).
[15] M. H. Lee et al. Nucl. Instrum. Methods A, in press (2005).
[16] R. A. Mewaldt et al., Proc. 29th ICRC, Pune, 1, 111 (2005).
[17] J. J. Engelmann et al., Astron. & Astrophys., 233, 96 (1990).
[18] D. Müller et al., Astrophys. J., 374, 356-365 (1991).
[19] K. Asakimori et al., Astrophys. J., 502, 278-283 (1998).
[20] A. V. Apanasenko et al., Proc. 26th ICRC, Salt Lake City, 3, 163, (1999).
[21] P. L. Biermann, Astron. & Astrophys., 271, 649 (1993).
[22] N. L. Grigorov et al., Proc. 12th ICRC, Tasmania, 5, 1746 (1971).
[23] K. Asakimori et al., Proc. 23rd ICRC, Calgary, 2, 21 (1993).
[24] M. Aguilar et al., Phys. Rep., 366/6, 331 (2002).
[25] T. Sanuki et al., Astrophys. J., 545, 1135, (2000).
[26] H. S. Ahn et al., Proc. 28th ICRC, Tsukuba, 4, 1853 (2003).
[27] M. J. Ryan, et al., Phys. Rev. Lett., 28 (15), 985 (1972).
[28] D. Mueller et al., Proc. 29th ICRC, Pune, 3, 89 (2005).
[29] P. J. Boyle et al., Proc. 29th ICRC, Pune, 3, 65 (2005).